

Gamma Veto Detectors in the KOPIO Experiment

Nicholas Lynden Graham

Thesis submitted to the faculty of the Virginia Polytechnic Institute and State University
in partial fulfillment of the requirements for the degree of

Master of Science
In
Physics

Marvin Blecher, Ph.D., Advisor
Mark Pitt, Ph.D.
Tatsu Takeuchi, Ph.D.

February 7, 2006
Blacksburg, Virginia

Keywords: Symmetry violation, kaon decay, scintillation detector

Gamma Veto Detectors in the KOPIO Experiment

Nicholas Graham

Abstract:

KOPIO is an experiment designed to search for the CP-symmetry-violating reaction $K_L^0 \rightarrow \pi^0 \nu \bar{\nu}$. Measurement of the branching ratio of this reaction would be the most precise measurement of the CP-violation parameters of the Standard Model to date. The $K_L^0 \rightarrow \pi^0 \nu \bar{\nu}$ reaction is exceedingly rare, with a branching ratio of $(2.6 \pm 1.2) \cdot 10^{-11}$. The rareness of this reaction means two things: 1) that we need prodigious numbers of kaons, and 2) that the multitude of “improper” decays will have to be screened out by means of a veto detector system being designed here at Virginia Tech.

This detector must be able to detect the passage of daughters of the undesired decay reactions (charged particles and gammas). It must be operational inside a magnetic field, and must have signal timing fast enough to accommodate the rate at which these decays occur. A detector consisting of alternating layers of scintillator and lead, with wavelength-shifting fibers embedded in the scintillator, provides the characteristics sought after. This paper presents methodology used in design and construction of this detector, as well as results of signal property tests, using both cosmic rays and gammas as event triggers. Also included is a discussion on extending the transmission range of the detector so the signal can be read by photomultiplier tubes resting outside of the sweeping magnet.

ACKNOWLEDGEMENTS

I would first and foremost like to thank my advisor, Dr. Marvin Blecher, for his guidance, understanding, and patience with me. I would also like to thank my friend, Dr. Athanasios Hatzikoutelis, for helping me do a lot of the physical work and analysis described in this paper, as well as keeping me focused on the big picture when I started to get bogged down in the details. Both of these men helped me tremendously, not only in the day-to-day work of the project, but in making the hectic life of a graduate student less troublesome.

CONTENTS

List of Figures.....	v
Chapter 1 – Theory.....	1
Chapter 2 – Detector Principles.....	2
Chapter 3 – Planning and Construction	
3.1 – Dark box construction.....	5
3.2 – Photomultiplier tube calibration.....	6
3.3 – Detector assembly.....	10
Chapter 4 – Prototype Testing and Results	
4.1 – PMT calibration with signal attenuation.....	13
4.2 – Cosmic ray and gamma response tests.....	15
Chapter 5 – Signal Transmission Extension Tests	
5.1 – Lucite as a coupling medium.....	19
5.2 – 5mm square clear/WLS optical fiber as a coupling medium...	20
5.3 – 1mm round WLS optical fiber as a coupling medium.....	24
Chapter 6 – Conclusions.....	28

LIST OF FIGURES

Fig. 1. Conceptual drawings of the decay region and sweeping magnet of the KOPIO detector.....	3
Fig. 2. Circuit diagram for prototype and slab signal tests.....	6
Fig. 3. Histogram detailing the PMT calibration process.....	8
Fig. 4. Calibration as a function of time.....	9
Fig. 5. ADC peak as a function of time.....	9
Fig. 6. Picture of one end of the detector module fiber bundle.....	12
Fig. 7. Example histogram used calibration, 12dB attenuation on signal output.....	14
Fig. 8. Histogram summary of results in cosmic ray response tests.....	16
Fig. 9. Cosmic ray signal histogram superimposed with background histogram....	17
Fig. 10. Histogram summary of results in gamma response tests.....	18
Fig. 11. Comparison of various combinations of Lucite length and wrappings in signal transport efficiency tests.....	20
Fig. 12. Attenuation functions for the far and near ends of 1.04m square wavelength shifting fiber.....	22
Fig. 13. Attenuation functions for the far and near ends of 1.20m square clear fiber.....	23
Fig. 14. Data from fiber attenuation length tests plotted with fitted approximation.....	25
Fig. 15. Difference between experimental data and approximation.....	26
Fig. 16. Chi-square fits for λ_S , λ_L , and α values.....	27

CHAPTER 1 - THEORY

In an instant, about fourteen billion years ago, the universe was born via the Big Bang. The Standard Model of Physics predicts that matter and antimatter were created in equal amounts in the explosion. So why, then, did the matter and antimatter not completely annihilate? Why is the universe now biased toward matter? The answer lies partly in charge-parity (CP) symmetry violation, which states that antimatter particles behave slightly different from their matter counterparts. According to physicist Andrei Sakharov, the asymmetry between matter and antimatter is dependent on CP violation; otherwise, for every process that changes the amount of matter in the universe, there is a process that changes the amount of antimatter such that the net effect is zero.

Many decay chains exhibit CP violation. Possibly the most famous of these is the decay $K_L^0 \rightarrow 2\pi^0$, first discovered by James W. Cronin and Val Fitch in 1964 at Brookhaven National Lab. KOPIO is an experiment that seeks to find and measure the branching ratio of the decay $K_L^0 \rightarrow \pi^0 \nu \bar{\nu}$. Measurement of this reaction is unique from that of other CP-violating reactions, in that it will provide the first direct measurement of the area of the unitary triangle, and thus will test the SM origins of CP violation. If the measured value of $B(K_L^0 \rightarrow \pi^0 \nu \bar{\nu})$ falls outside of $(3 \pm 2) \cdot 10^{-11}$, the range predicted by the SM, it is an indicator of new physics.

CHAPTER 2 - DETECTOR PRINCIPLES

The $K_L^0 \rightarrow \pi^0 \nu \bar{\nu}$ reaction is notoriously difficult to detect, as there are many decay chains for the K_L^0 that result in a π^0 , or gammas that can emulate a π^0 , which is the only particle in $K_L^0 \rightarrow \pi^0 \nu \bar{\nu}$ that can be detected. Therefore, a means of ensuring that the detected π^0 is the only particle emitted in the decay is necessary. This is done by time-of-flight analysis, which determines the K_L^0 momentum. The π^0 can be transformed to the center-of-mass frame of the K_L^0 , and kinematic constraints can be applied to suppress detection of background decays. Background rejection is done by means of high-sensitivity photon vetos and angle, position, and energy measurements. By tracking the path and energy of each photon detected, one can determine whether there is a π^0 with the correct kinematics.

The beam of K mesons used in this experiment will be provided by the Alternating Gradient Synchrotron (AGS) at Brookhaven National Lab. The AGS is capable of providing large numbers of kaons in the energy range needed by KOPIO. The beam will be structured in 200ps pulses at a rate of 25MHz (40ns pulse separation). The decay region of the detector will be highly evacuated, to suppress neutron-induced π^0 production. Only events bearing the signature of a single kaon going to two photons are accepted. The timing, position, and angles of the photons from $K_L^0 \rightarrow \pi^0 \nu \bar{\nu}$ are obtained using a preradiator, while the energy is obtained in combination with a Shashlyk calorimeter behind the preradiator. Backgrounds within the decay region are detected and vetoed using a barrel veto detector with lead/scintillator modules that surround the decay region. A conceptual drawing can be seen in Figure 1.

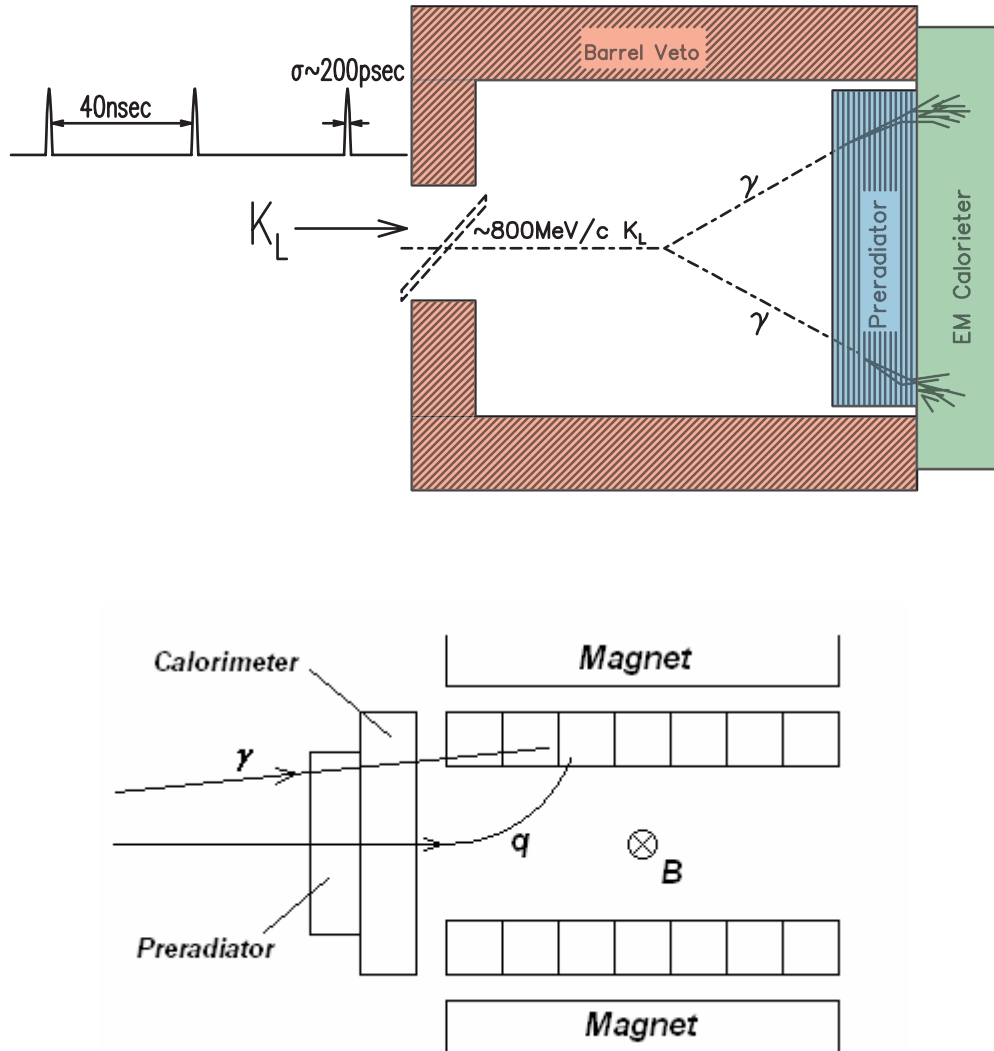


Figure 1: Conceptual drawings of the decay region and sweeping magnet of the KOPIO detector.

Occasionally, photons and charged particles will leave the decay region through a beam hole in the preradiator and calorimeter. If this occurs, the events must be vetoed by the downstream veto detectors, some of which are being designed here at Virginia Tech. The downstream veto detectors will be placed inside a sweeping magnet, so that any charged particles that result from decaying kaons will be swept into the detector.

The detector modules are made of alternating layers of plastic scintillator and lead. Grooves are cut lengthwise into the scintillator, allowing green wavelength-shifting (WLS) fibers to be placed without disrupting the laminar geometry of the scintillator and lead. The scintillator releases a pulse of blue light whenever a charged particle passes through it. This light travels in the scintillator until it is trapped by the fibers. The fibers absorb the blue light and emit green light; this is done so that the signal can be trapped and carried by the fiber via total internal reflection. The lead is present to convert gammas to charged particles that the scintillator can “see.”

CHAPTER 3 - PLANNING AND CONSTRUCTION

To ensure that the data from the phototubes used in the testing would not be corrupted by room light, a light-tight box was constructed. This box consisted of a lid which fit snugly over a raised surface where the items being tested would rest. The lid was made of a wooden frame, 6m x 40cm x 20cm in dimension. To the inside of the wooden frame was stapled first a layer of black opaque plastic, then a layer of black felt. A loose layer of black felt was used for wrapping the test items before lowering the box onto the support. To test the light tightness, a PMT was placed inside the dark box and turned on. The PMT signal showed no difference with window light only and overhead room lights on, indicating a light-tight environment.

Testing of the light output and timing of the detector module was done using cosmic rays. To avoid false signatures in the data, a cosmic ray telescope was made. The assembly consists of three photomultiplier tubes (PMTs) attached directly to scintillator panels via Lucite lightguides, and wrapped in black electrical tape to ensure light tightness. Two of these PMT assemblies were placed under the dark box, and one was placed over the dark box so that the scintillator panels were vertically aligned. For an event to be counted in the analog-to-digital converter (ADC) and time-to-digital converter (TDC), the telescope and detector PMTs must receive a signal within a 50 ns window, indicating a charged particle passing vertically through the entire array. The circuitry for the detector can be seen in Figure 2.

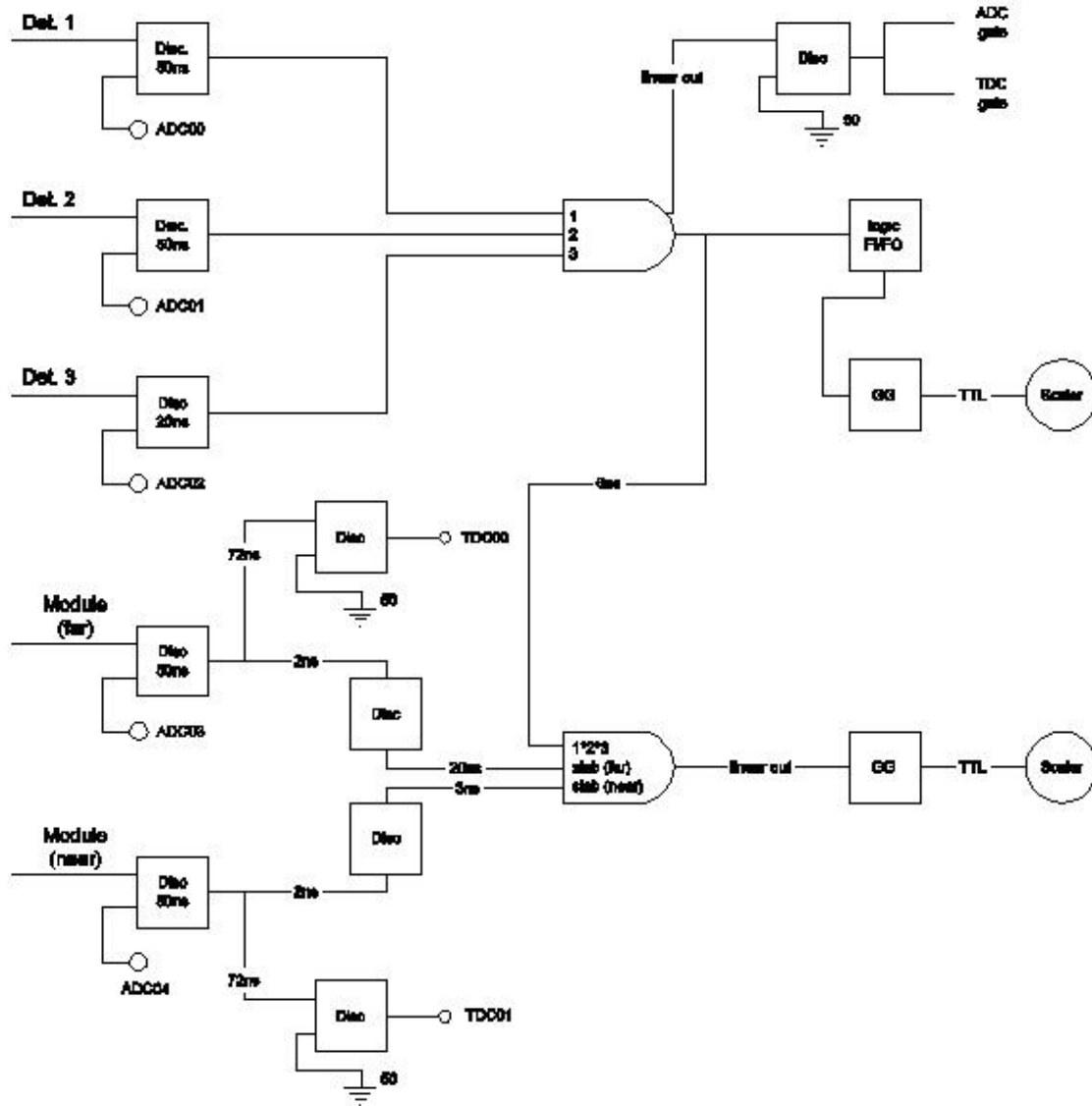


Figure 2: Circuit diagram for prototype and slab signal tests. The detector makes use of a 3-way coincidence to ensure that the events recorded are cosmic rays.

Before construction on the detector module was started, we first calibrated the photomultiplier tubes used in the experiment. This was done by means of a small bundle of WLS fibers, one end of which went to the PMT in question. Light from a blue LED was pulsed at a frequency of 1 kHz on top of this bundle. The fiber shifted the blue light to green and transmitted it into the PMT. The voltage to the LED was adjusted to give a

peak around 700 channels in the ADC, and then attenuated by one decibel to give the single photoelectron peak (see Figure 3 for an example histogram). The SPE peak was fitted to a Gaussian function to find the mean.

The next tests done were to determine the time stability of the PMT calibration. The high voltage to the tubes was turned on for a sustained amount of time. Data runs were taken at various elapsed times, with the LED at the single photoelectron level, and the resulting histograms were fit to a Gaussian function to find the mean. Results show that the calibration is stable after the two hour mark (see Fig. 4).

To determine the time stability of the amount of light received by the phototube, a similar process was used, except the voltage on the LED was increased. Runs were taken at various elapsed times. Results show that the peak remains stable. The PMTs were not turned off, nor was the light source moved, between runs (see Fig. 5).

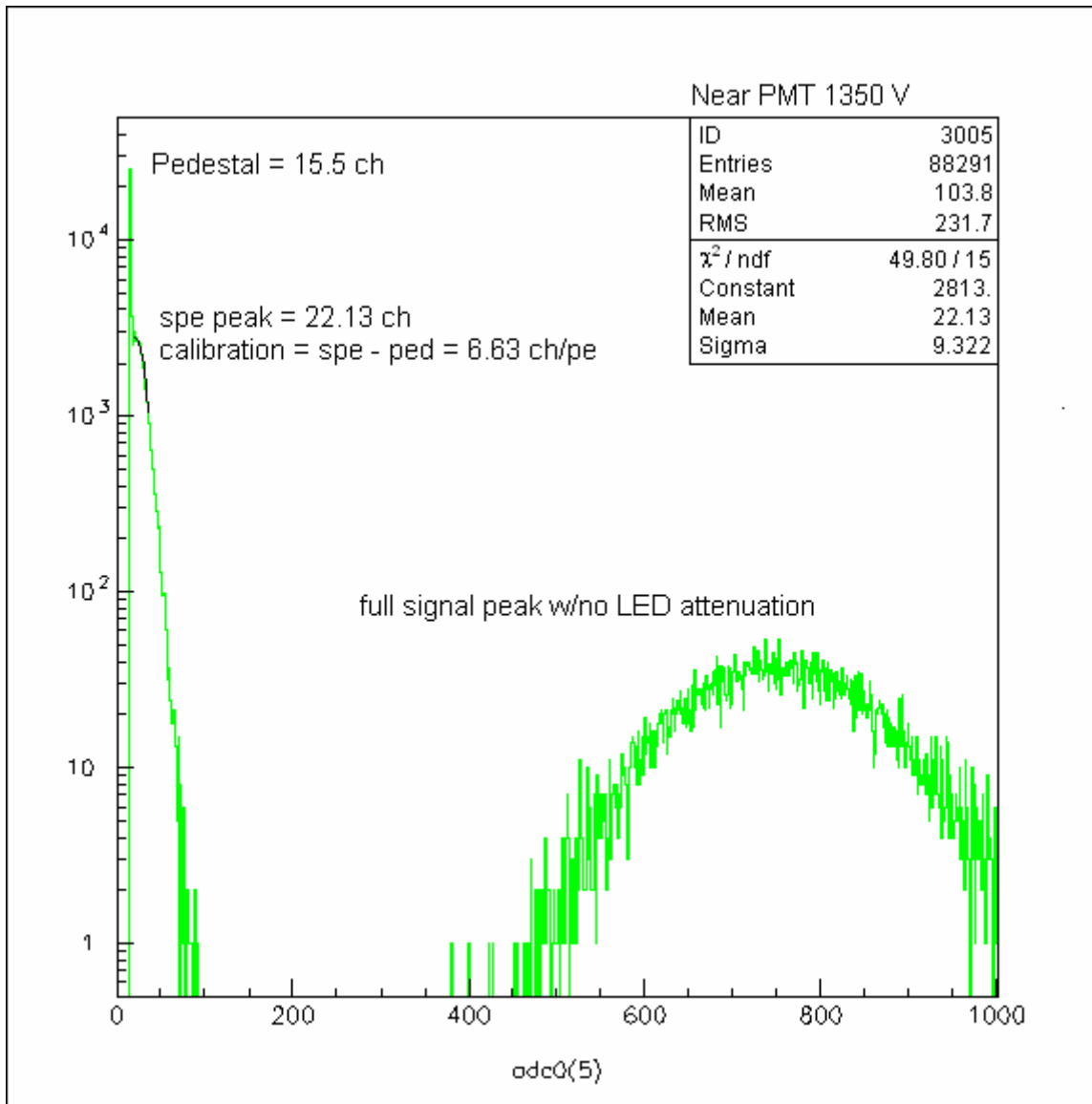


Figure 3: Histogram detailing the PMT calibration process.

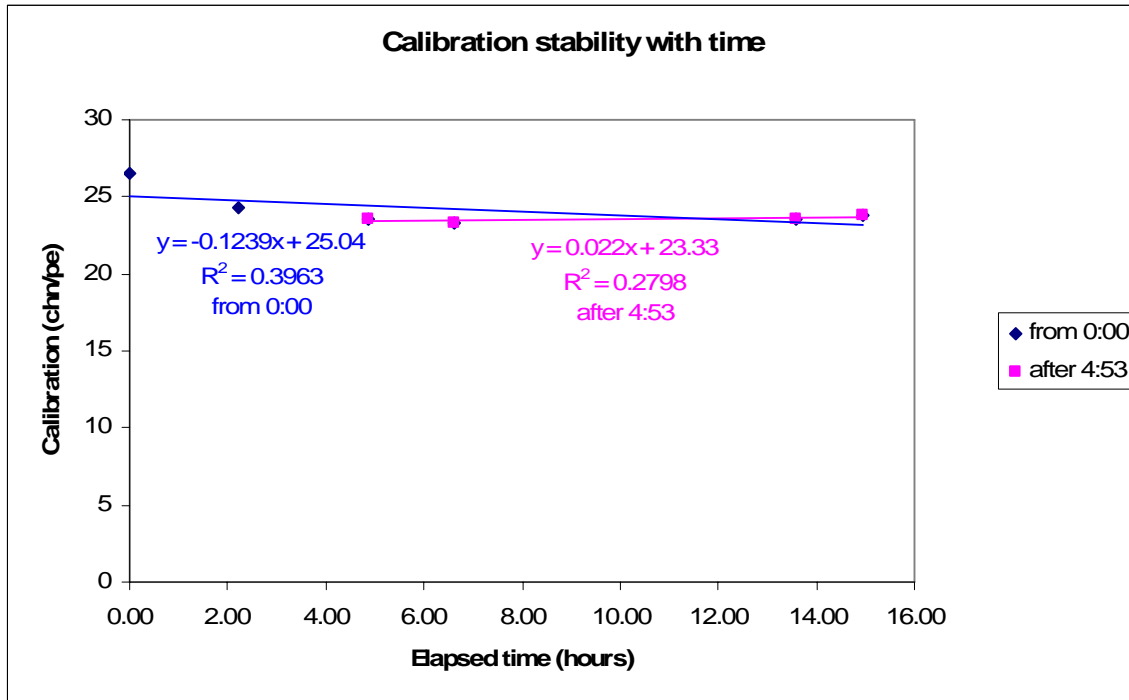


Figure 4: Calibration as a function of time. The calibration appears to stabilize once the phototubes have been on for two hours.

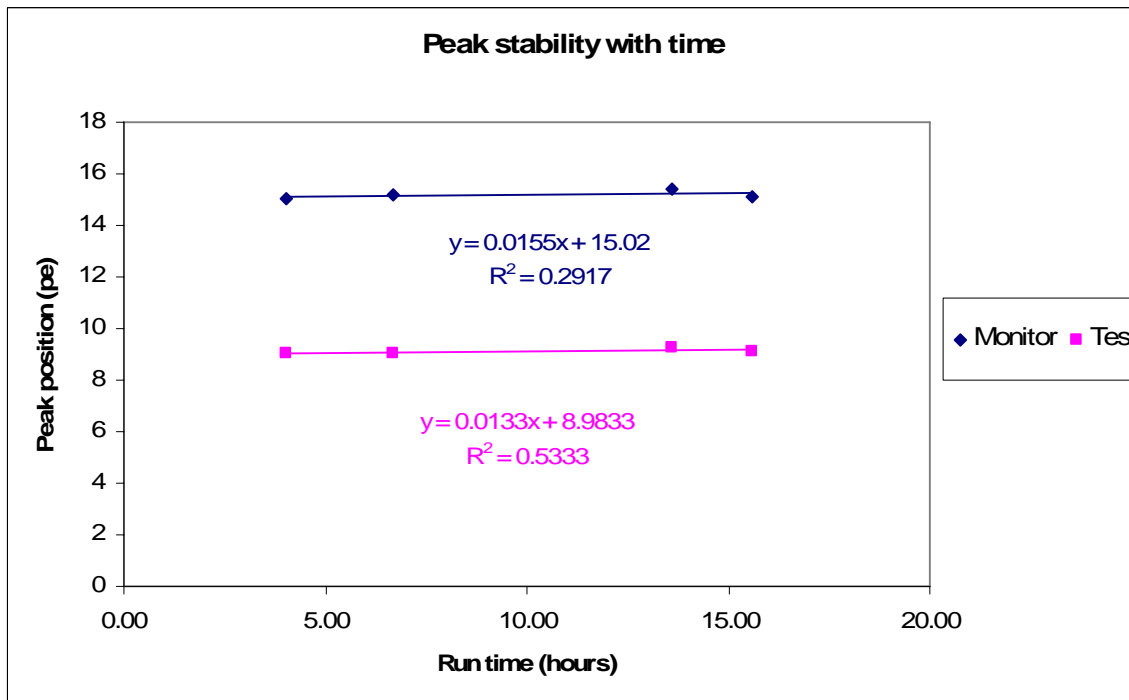


Figure 5: ADC peak as a function of time. Once the phototubes have been on for four hours, the amount of light received by the phototubes remains stable.

Once the calibration of the phototubes was determined to be stable, construction of the single slab/fiber assemblies began. Three coupling media (air, optical grease, and optical cement) and four types of fiber (Bicron and Kuraray single- and multi-clad fibers) were investigated for light retention in cosmic ray tests. The tests were done using fibers placed into the grooves with the chosen coupling medium. The fibers were then bound at the ends using Teflon tape and plumbing hose, and the ends of the bundles were polished using a rotary sander at 150 rpm, first with 200 grit sandpaper, then with 400, then 1600. Water was applied as necessary to keep the paper wet. The slab was then placed in the dark box and centered within the cosmic ray telescope. PMTs were affixed to the ends of the fiber bundles, using optical grease as a coupling. The PMTs were switched on, the assembly was observed to ensure proper detection of cosmic rays, and was left to collect data overnight. It was found upon analysis that the most light came from the combination of Kuraray multi-clad fibers in optical cement (see KOPIO Technote 084).

To begin assembly, one 15cm x 0.5m slab was prepared by cleaning the surface and the grooves with alcohol and high-pressure air. The optical cement was mixed and put into a syringe with a narrow tip, dispensed into the grooves of the slab, and fibers were laid in the grooves on top of the cement. The fibers were then tacked down with three small dots of superglue each, one in the middle and one at each end, to ensure that they did not rise up from the grooves before the cement had dried. Excess cement was then cleared away using a rubber squeegee blade.

Once the cement had dried, the fibers at each end were gathered and bound tightly with Teflon tape and plumbing hose. A high-speed rotary saw was used to cut the excess from the ends of the bundles, and to make the length of the bundles equal. The ends of

the fibers were then polished using a variable-speed rotary step motor at 160 rpm and sandpaper. The first step in polishing was 15-20 minutes with 240 grit sandpaper; the second step was 20-30 minutes with 400 grit sandpaper; the third step was 45-60 minutes with 1600 grit sandpaper. The sandpaper was lubricated with water as needed to keep dust from accumulating.

Once the ends were polished, each bundle was placed into the small end of a plumbing size reducer. The fiber bundle was greased and placed against the face of the PMT, which was then inserted into the large end of the reducer and taped to form a stable support structure for the fiber coupling. The slab and tubes were then placed into the dark box and testing was done to determine signal and timing characteristics of the single slab assembly. The slab was shown to have an average total light output of 61 pe/event, and a timing resolution of 1.3ns. Simulations predict an energy deposit of 1 MeV per slab per event, our experimental threshold of 67 keV corresponds to a 4pe signal, which is easily detected by the PMTs.

To construct the prototype detector module, nine more single-slab assemblies were constructed in the manner detailed above, except the fibers were not bound at the ends. 2.5mm thick lead sheets were cut in the same dimensions as the scintillator slabs, and painted with a coat of black primer for safe handling during the construction. One scintillator slab was placed fiber-side up into a stabilizing framework made by the machine shop. Freshly-mixed Hysol epoxy was applied to a lead panel, which was then pressed onto the fiber side of the slab. Weights were placed on the lead, and the adhesive was left to dry over several days. This process was repeated eight times, yielding nine slab/lead pairs and one single slab assembly. The slab/lead pairs were then glued

together in sets of three using the Hysol and weights, and the resulting three parts were glued together in a similar manner. The tenth slab was then glued on top of the ninth sheet of lead to finish the central part of the detector prototype.

Once the Hysol had had sufficient time to cure (approx. one week) the loose fiber ends were bound tightly with Teflon tape and two layers of plumbing hose. The excess fiber at the ends was trimmed with a high-speed rotary saw to give the fibers on each side of the module equal length and a flat surface. The ends were then polished using rotary step motors and sandpaper disks of grits 240, 400, and 1600, and then finished with soft pumice polishers. This treatment resulted in a good flat surface, with high light yield (see Figure 6).



Figure 6: Picture of one end of the detector module. Room light was dimmed for the picture to emphasize the high light output of the fibers.

CHAPTER 4 - PROTOTYPE TESTING AND RESULTS

For the cosmic ray tests of the prototype, the PMTs were set at 1350 volts for the left and 1400 volts for the right. Single-slab testing with the PMTs at this voltage level yielded a total light output of 61 photoelectrons, which showed in the histograms generated by the MIDAS data acquisition software as a peak around 800 channels at each end of the fiber. Because the ADC has an upper threshold of 1130 channels, the result from cosmic ray tests on the 10-slab prototype would be almost entirely overflows. Therefore, the signal from the PMT must be attenuated before inputting it into the ADC; this implies that a new calibration must be done.

Calibration of the attenuated signal was done similarly to before: a short bundle of 12 WLS fibers was coupled to the PMT in question, while blue light was pulsed at 1kHz on top of the fibers. However, after attenuating the signal by 12dB, the single photoelectron peak dropped to such a low channel in the histogram that it was indistinguishable from the pedestal. Therefore, two runs were taken: one with no attenuation, and one with 12 dB attenuation. For the run with no attenuation on the PMT, the LED voltage was tuned to a level that gave a full signal peak at around 800 channels in the ADC, then the LED voltage was step-attenuated by 1dB to show the single photoelectron peak. This gives the total number of photoelectrons for the full voltage signal with no attenuation. Then, removing the attenuation on the LED voltage, 12 dB of attenuation was placed on the PMT signal and a full signal peak was read by the ADC. Using the number of photoelectrons found in the first data run, the calibration of the PMT with attenuation was then found by dividing the peak location in channels by the number

of photoelectrons in the signal. The near (left) PMT was found to have a calibration of 1.70 ch/pe, while the far (right) PMT was found to have a calibration of 2.01 ch/pe. An example histogram can be seen in Figure 7.

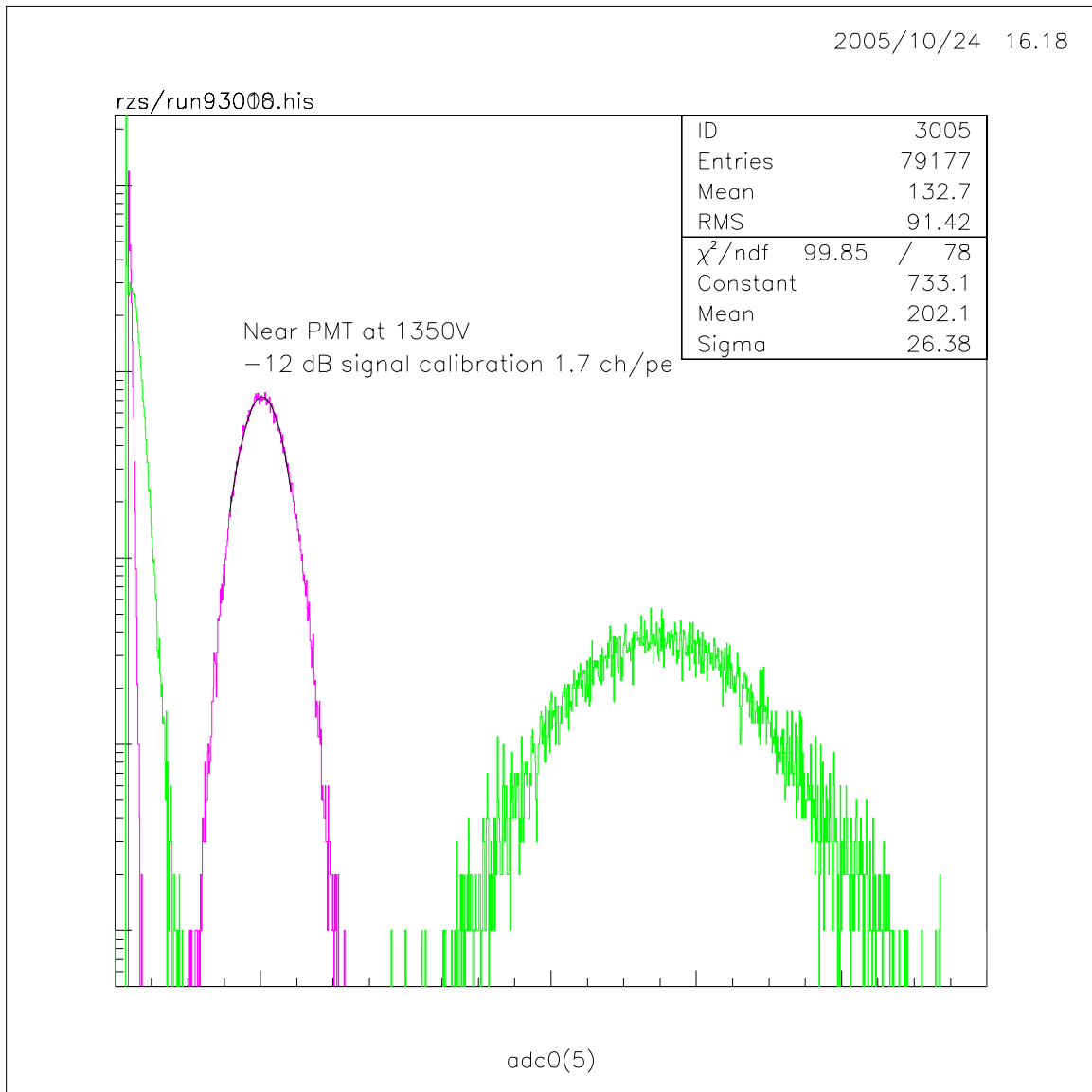


Figure 7: Example of calibrating PMTs with 12dB attenuation on signal output.

The method used for testing the signal and timing response of the assembled prototype was similar to that used for the single-slab tests. The prototype assembly was moved onto the base of the dark box and centered within the cosmic ray telescope, the PMTs were coupled to the ends of the fiber bundles using optical grease, and the lid of the box was secured. The tubes were turned on and MIDAS was started and left to collect data overnight. Analysis of the resulting histograms showed a signal strength of 197pe/event from the left PMT and 210pe/event from the right PMT for a total light output of 410pe/event, less than the expected 610pe/event (10 slabs x 61 pe/slab). This difference is most likely due to the inherent difficulties of polishing 190 fibers in a bundle, compared to polishing 19. With a total energy deposition of 9.2 MeV/event (obtained through simulation), this corresponds to a 90 keV energy threshold per 4 pe. Timing of the cosmic ray signal was also found, using the TDC histograms. The timing resolution corresponding to cosmic ray events was found to be 0.88ns (σ), on average. A summary of the ADC and TDC histograms can be seen in Figure 8.

A measurement of the background was taken by removing two of the telescope detectors from the coincidence and letting the ADC and TDC gates trigger on the dark current signal of the third telescope detector. Superimposing the background plot and the signal plot, it is obvious that the background does not contribute to the signal (see Figure 9).

Once the cosmic ray tests were done, the telescope was modified to allow testing of the prototype's response to gamma rays. This was done by replacing the top telescope detector's scintillator panel with a larger scintillator panel and lightguide, and placing it into anti-coincidence with the signals from the PMTs on the prototype. Analysis shows a

total signal strength of 401 pe/event (corresponding to cosmic rays) and a timing resolution of 0.6 ns (σ). The response of the detector to gammas can be seen in the higher activity level in the lower end of the histograms; however, it appears as though the geometry is such that cosmic rays are still detected. Had KOPIO been continued, a more thorough test of gamma veto efficiency, using a calibrated gamma source, would have been done at Brookhaven. A summary of the gamma ray tests can be seen in Figure 10.

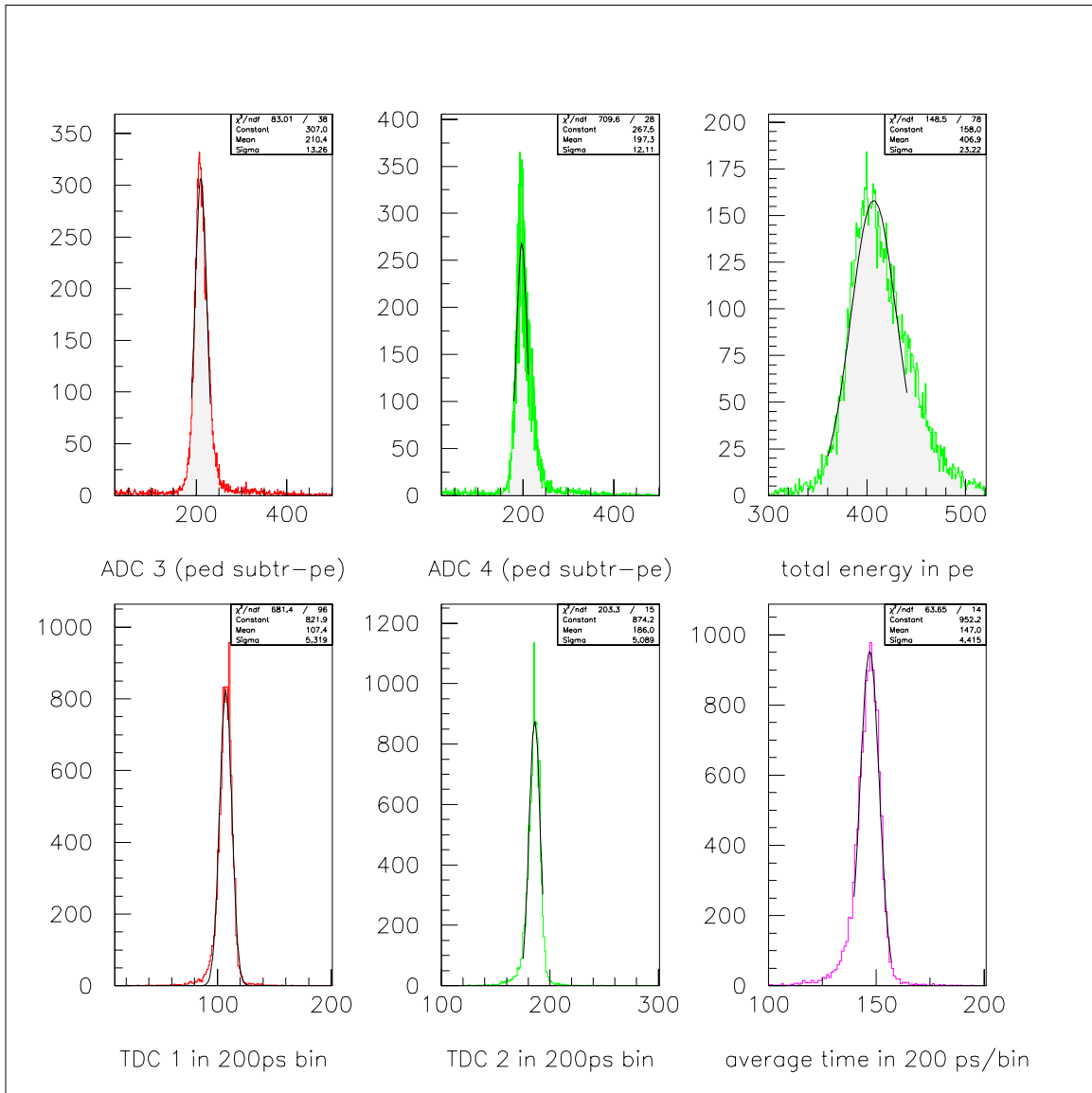


Figure 8: Summary of results in cosmic ray response tests. Total signal strength was 410pe/event, and the timing resolution was 0.88ns (σ).

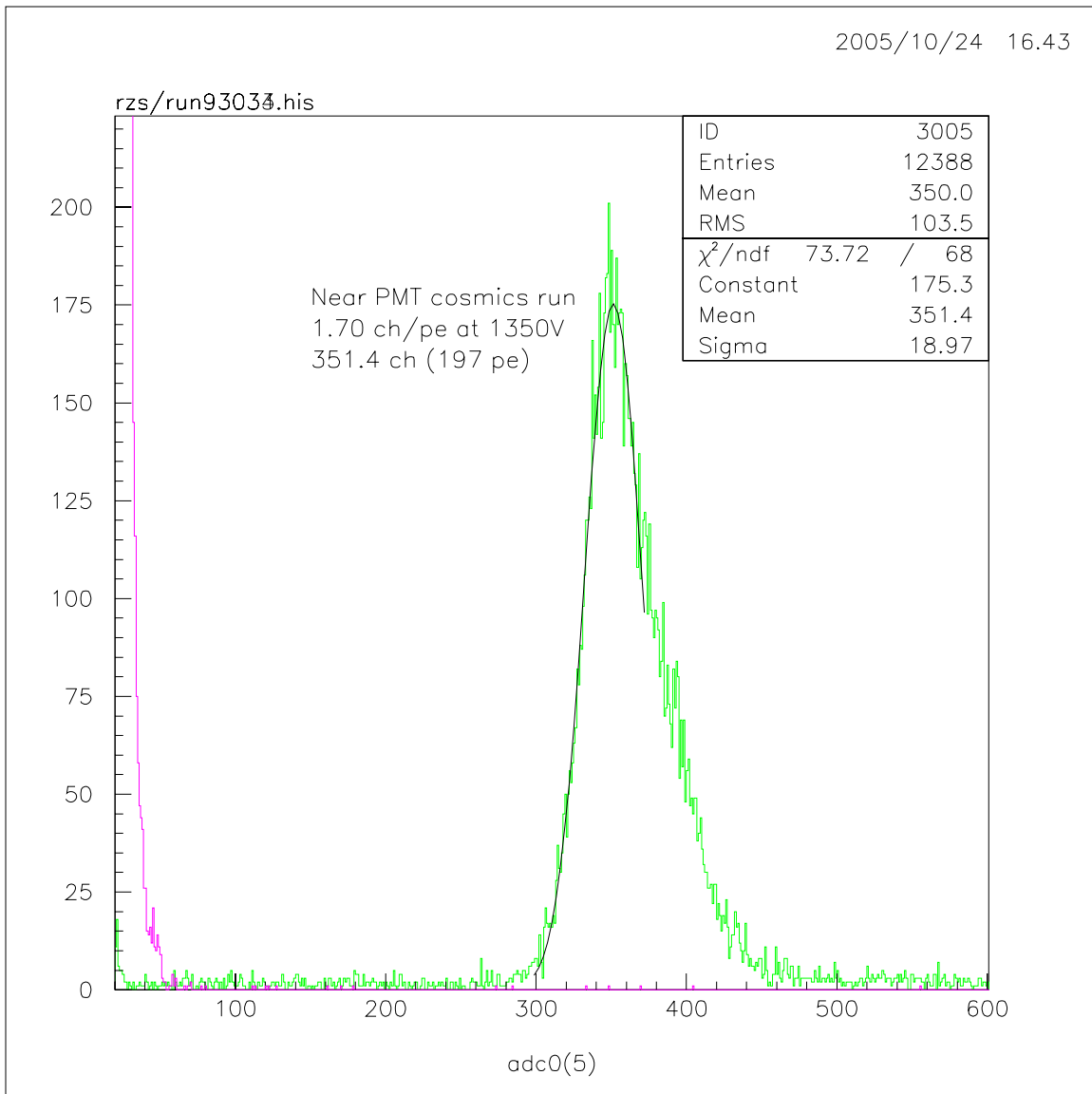


Figure 9: Cosmic ray signal histogram and background histogram superimposed. The background does not contribute to the signal peak at all.

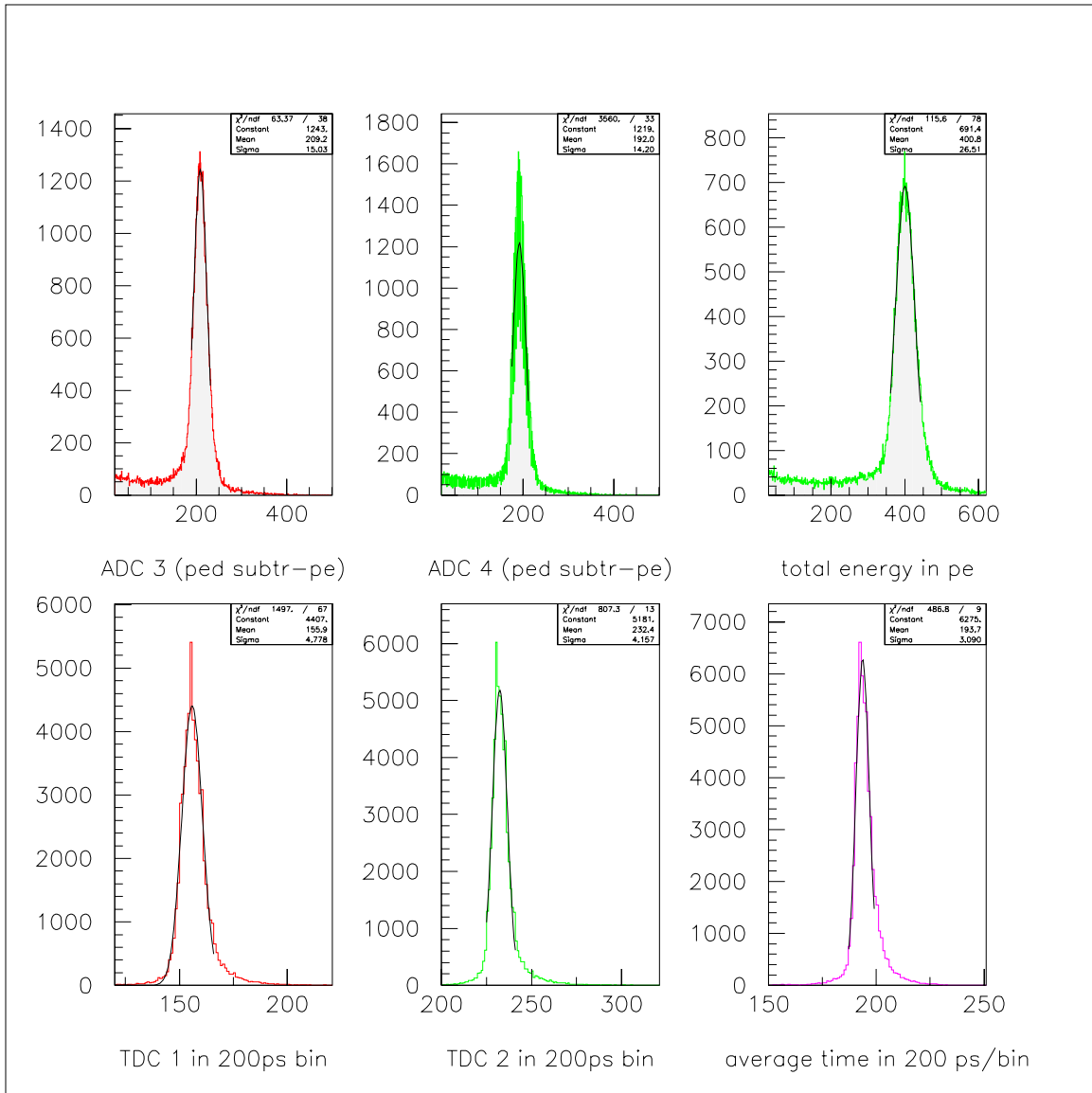


Figure 10: Summary of results in gamma response tests. Total signal strength was 401pe/event, and the timing resolution was 0.60ns (σ).

CHAPTER 5 - SIGNAL TRANSMISSION EXTENSION TESTS

Since phototubes are to be used in the assembly, we must have some method of transmitting the light outside the magnetic field in which the modules will be placed. Several methods for this were investigated, including optical coupling with Lucite and clear and WLS optical fibers of varying dimension. Also considered was construction of the single slab assemblies using very long WLS fibers.

The first method tried was coupling the WLS fibers from the slab to a two-inch-diameter Lucite cylinder, which is wrapped in one of several different wrappings. For these tests, we shined a blue LED on a short bundle of 12 fibers, laid out flat. One end was bundled and went directly to the phototube (the monitor), while the other end was bundled and coupled using optical grease to the end of the Lucite cylinder. The other end of the Lucite cylinder was coupled to a phototube. The LED was not located at the center of the fiber bundle, so the first data run was taken with no Lucite (both ends of the fiber bundle straight to phototubes) to determine the scaling factor for the fibers; every run after that was calculated using this scaling factor.

Runs were taken using a two-foot Lucite cylinder, wrapped in black paper, mylar (single or multiple wrappings), and Tyvek (single and multiple wrappings), as well as a one-foot cylinder with the same wrappings, as well as with white paint. The best results were achieved using a double wrapping of Tyvek, resulting in an attenuation length of 2.46m. A summary of the results can be seen in Figure 11.

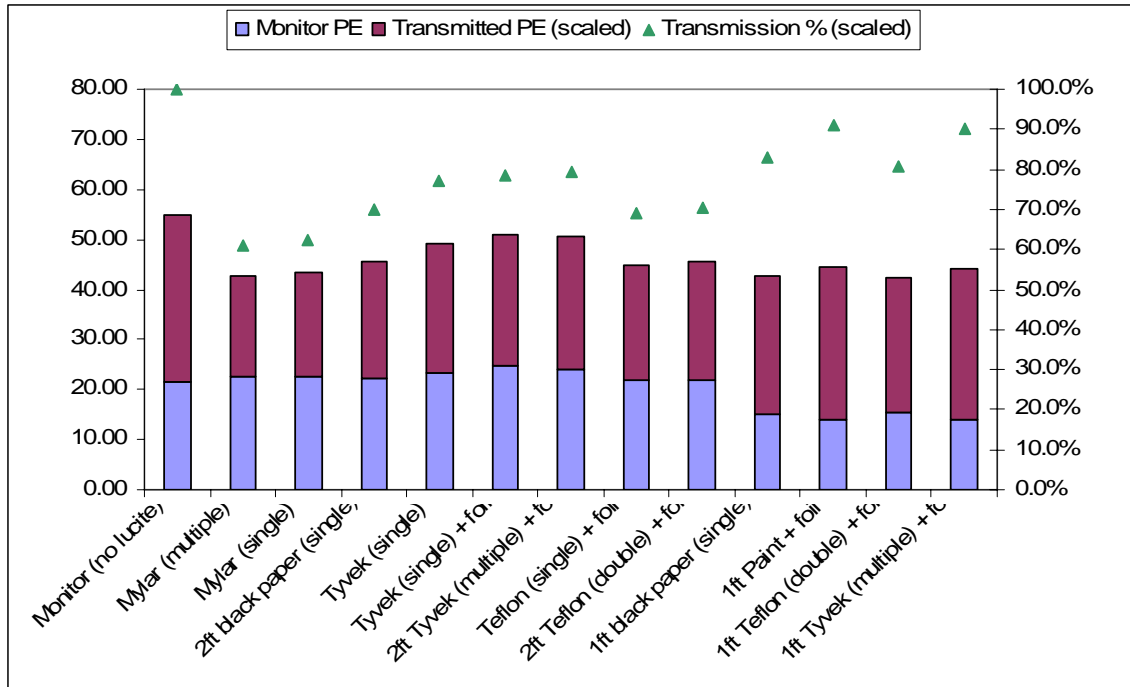


Figure 11: Point-by-point comparison of various wrapping/lengths of Lucite. The "monitor" data is used to normalize the transmitted light to that of the side with no Lucite.

Of the available wrappings, multiple layers of Tyvek returned the greatest consistency and amount of light. However, due to the short attenuation length of Lucite, compared to other methods, for instance, long lengths of WLS fibers, caused us to discard Lucite for transmitting the light outside the magnetic field.

Another method tried was coupling the WLS fiber bundles from the slab to single 5mm square fibers. Both Bicon multiclاد WLS fiber and Bicon multiclاد clear fibers were tested. The square fibers were cut with a high-speed rotary saw, and then polished first with 400 grit sandpaper on a rotary base, then with a soft buffing pad, soaked in water and covered in a very fine grit paste. This produced a "reflective surface" on the face of the fiber. The bundles were then coupled to the square fibers by means of a Plexiglas connector that was created in the machine shop. The cap of the connector is

screwed onto the base, creating a “clamp” for the fibers. Optical grease was used as the coupling medium.

WLS fiber is characterized by two attenuation lengths: at short distances, the green light emitted by the fibers can be reabsorbed, and at long distances, normal attenuation occurs. For the large square fiber tests, the length of the fiber being tested are short enough that the primary means of attenuation is due to reabsorption; the normal attenuating component can be neglected.

The first tests of square fiber were done using a 1.04-m-long square WLS fiber. An attenuation length test was performed using a white LED pulsed at various points on the fiber. The light transmitted through each end was read by a phototube, and the attenuation lengths were to be determined. However, these tests revealed an asymmetry in the amount of light transmitted through each face, presumably due to irregularities in polishing. It was then decided that finding the attenuation function (in decibels) for each end of the fiber, rather than the attenuation length, was preferable for our purposes. The amount of light transmitted through each end of the fiber was normalized to one end, and transmission percentages were found. These percentages were then converted to the decibel attenuations used in finding the functions. The attenuation function for the far end of the fiber was found via linear regression in Excel to be $\Delta I = -5.37(\text{dB}/m) \cdot x + 0.94(\text{dB})$, and that of the near end was found to be $\Delta I = -5.15(\text{dB}/m) \cdot x - 0.30(\text{dB})$ (see Fig. 12).

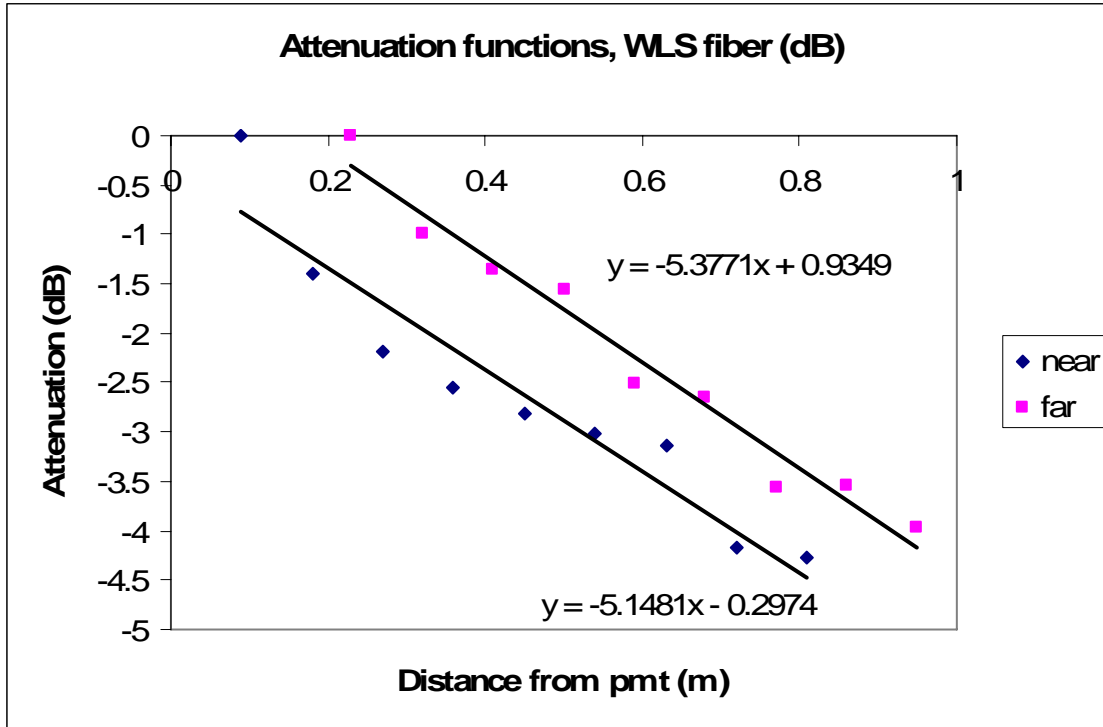


Figure 12: Attenuation functions for the far and near ends of the 1.04m square WLS fiber.

Also performed was a test to determine the loss in the connection between square and bundled fibers, using the connector. In this test, a 1.04-m length of square WLS fiber was coupled to a 1.01-m length of 12 bundled 1-mm WLS fibers. To determine the initial light input into the connection, a blue LED was pulsed onto the bundle at the midpoint, and the output at each end was read by the PMTs. The square fiber was then coupled to the far side of the bundle, using the connector, and the other side of the fiber was coupled to the far PMT. The LED and near side of the bundle were not moved. The light output from the bundle was 67.8 pe, while the light from the square fiber was 17.3pe (15.3 pe after normalization). The total signal drop from 52 pe to 15.3 pe is -5.3 dB (70.6%). Using the attenuation function for the far side of the fiber, we find a signal drop

of -4.66 dB (65.8% of light that enters the fiber, or 56.8% of total initial light from the bundle), indicating a signal drop in the connector of -0.64 dB (13.7%)

The same tests were repeated using the clear square fiber. Attenuation function analysis was done, similarly to with the WLS fiber. These tests yielded attenuation functions of $\Delta I = -4.87(dB/m) \cdot x + 0.84(dB)$ for the far end of the clear fiber, and $\Delta I = -6.25(dB/m) \cdot x + 0.51(dB)$ for the near end. This graph may be seen in Fig. 13.

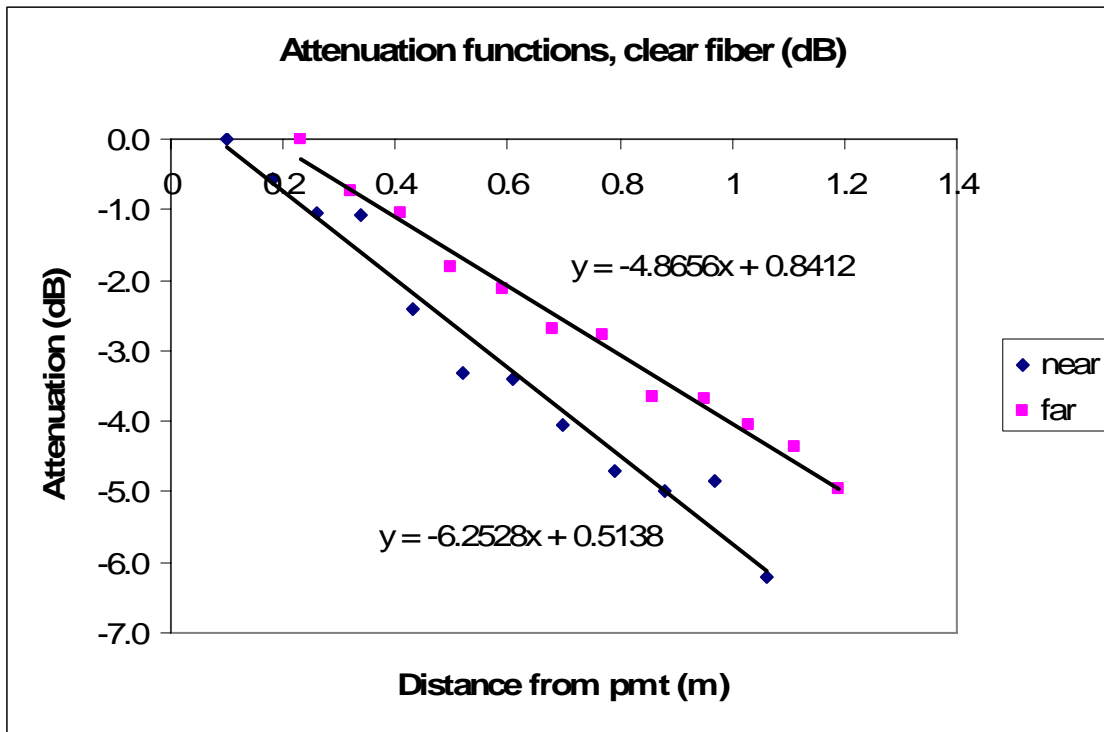


Figure 13: Attenuation functions for the far and near ends of 1.2m square clear fiber.

Attenuation length of the clear square fiber is quoted from the manufacturer’s literature to be 10-12 meters, which would correspond to an attenuation function with a slope between -0.36 dB/m and -0.43 dB/m. This is sharply at odds with the values of -4.87 dB/m and -6.25 dB/m obtained in the analysis. This may be due to the inability of the clear fiber to respond to light shined perpendicularly to the axis of the fiber.

The final tests were done to determine the fitness of long WLS fibers in carrying the light outside the magnetic field. To do this, twelve six-meter-long fibers were bundled together and the ends were polished. The fibers and tubes were contained in a light-tight environment. On the first 1.5m section of the fibers, an LED was used to pulse white light at various positions. The light transmitted to each end of the fiber was recorded in units of photoelectrons.

The WLS fibers used in the veto detector modules are characterized by two attenuation lengths, similarly to the square WLS fiber. Assuming an initial light intensity of $2I_0$ resulting from the LED shining on the fiber bundle, the intensity after attenuation is shown in Equation 1:

$$\begin{aligned} I_N &= I_0 \left(A e^{-x/\lambda_s} + B e^{-x/\lambda_L} \right) \\ I_F &= I_0 \left(A e^{-(L-x)/\lambda_s} + B e^{-(L-x)/\lambda_L} \right) \end{aligned} \quad (1)$$

where L is the length of the fiber bundle, x is the distance from the LED to the near end of the fiber bundle, and λ_L and λ_S are the long distance and short distance attenuation lengths. I_N and I_F are the light intensities at the near and far ends of the fiber bundle, respectively.

To account for the fluctuations in I_0 between data runs, we take the ratio seen in Equation 2:

$$\frac{I_F}{I_N} = \frac{e^{-(L-x)/\lambda_s} + \alpha e^{-(L-x)/\lambda_L}}{e^{-x/\lambda_s} + \alpha e^{-x/\lambda_L}}, \text{ where } \alpha = B/A. \quad (2)$$

Chi-squared minimization (via solver in MS Excel) is used to find the λ_L , λ_S , and α values, $\lambda_S = 0.88$ m, $\lambda_L = 5.83$ m, and $\alpha = 1.058$; the latter of the attenuation lengths is adequate for KOPIO. Manual chi-squared mappings were made around each of these

values to ensure sufficient minimum and depth. The results of the fits are shown in Fig. 14. Deviations from the fit are shown for each data point in Fig. 15. The chi-squared mappings are shown in Fig. 16.

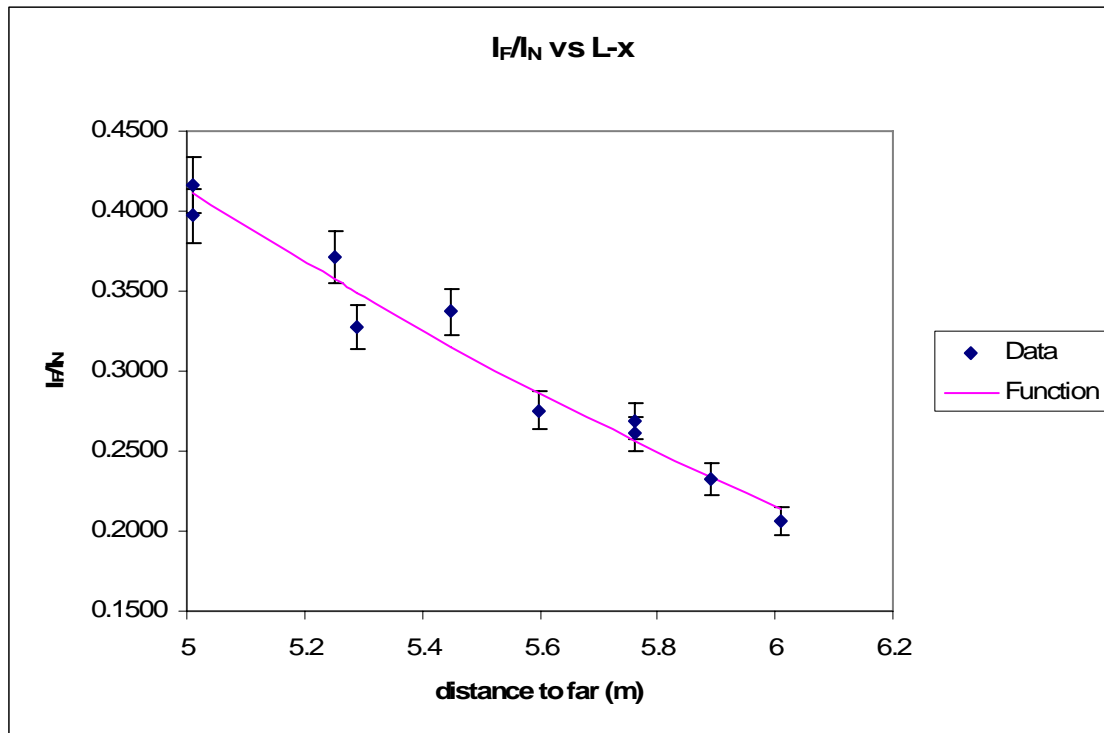


Figure 14: Data from fiber attenuation length tests plotted with the fitted function (Equation 1). Measurement errors are $1\text{pe}/30\text{pe}$ or about 3%. Fitted values of the parameters in Equation 1 were found using chi-squared minimization.

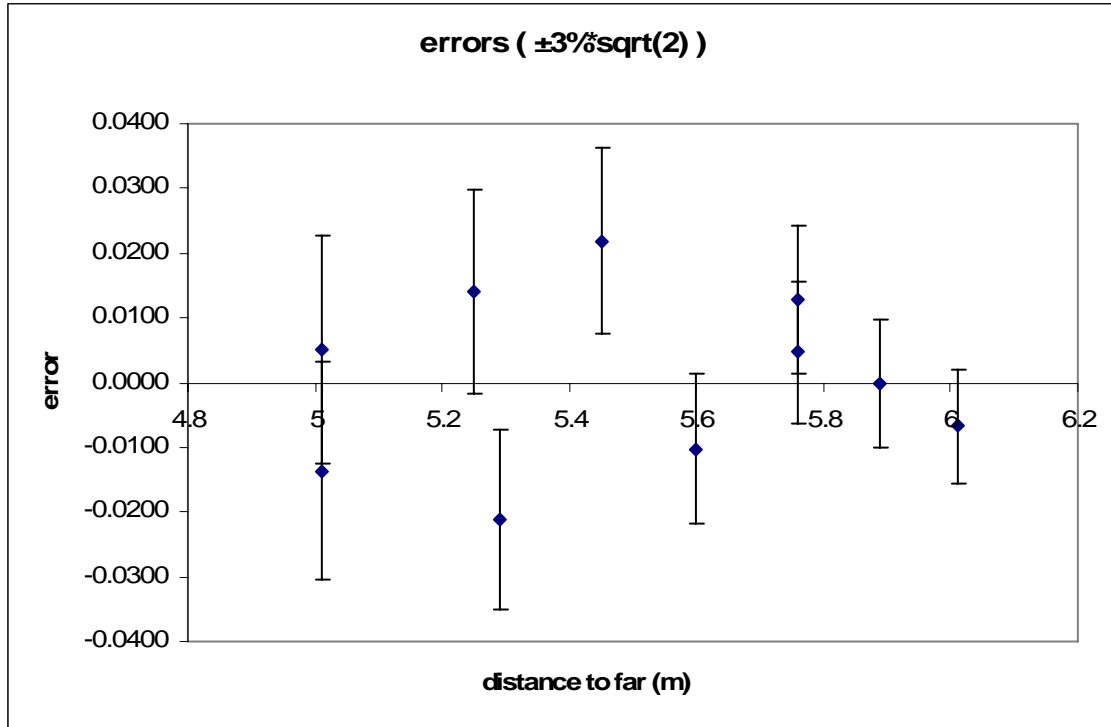


Figure 15: Difference between experimental data and ideal function. Error bar limits are $3\% \cdot \sqrt{2}$ of the data.

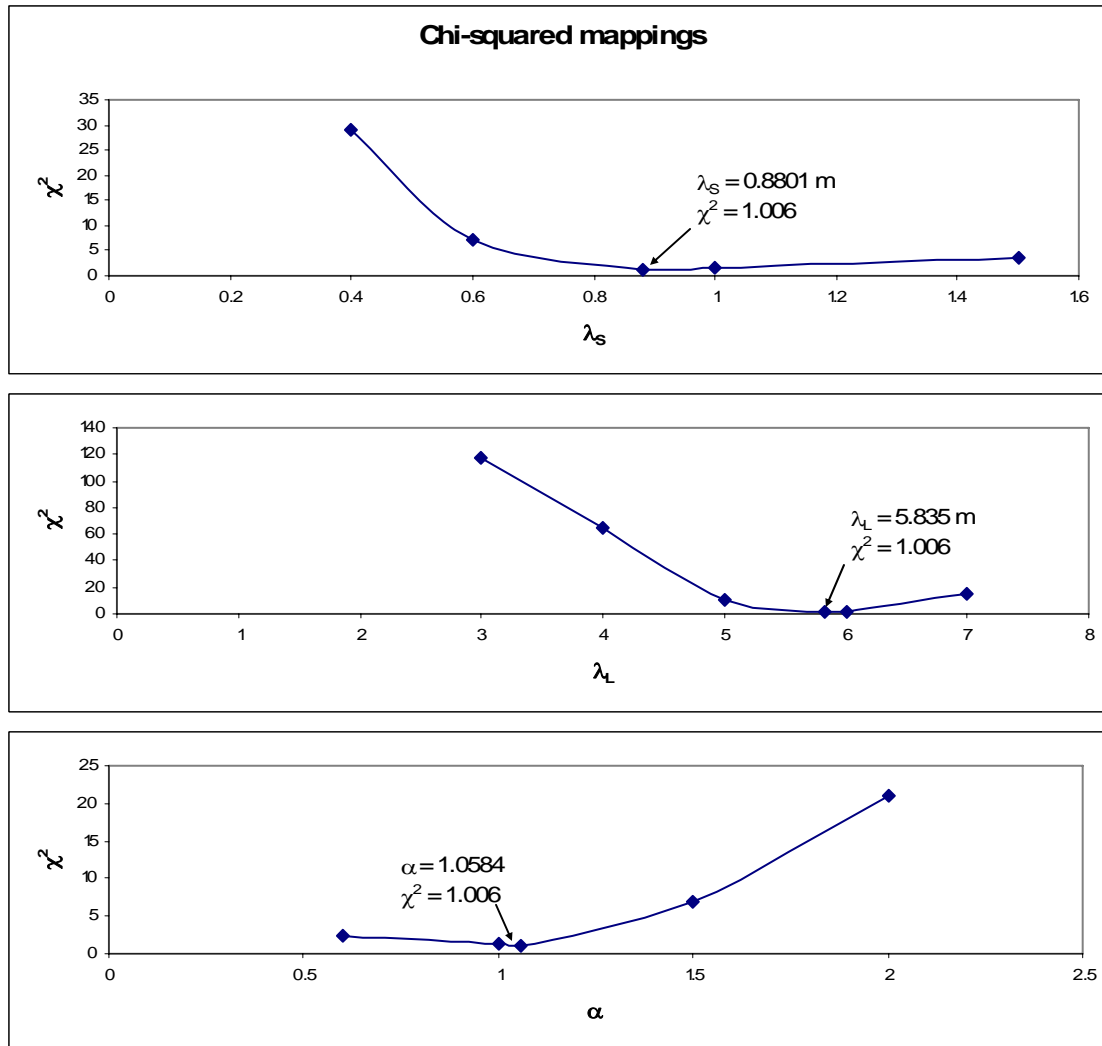


Figure 16: Mappings of chi-squared vs. λ_S , λ_L , and α . Minimization gives values of $\lambda_S = 0.88$ m, $\lambda_L = 5.84$ m, and $\alpha = 1.0584$ (indicating roughly equal attenuation by self-absorption and normal means).

Further testing on this matter would have been carried out, had KOPIO not been terminated. The found value for the attenuation length of the clear square fiber (0.8 m) was sharply at odds with the value quoted in the accompanying literature (10-12 m). The best option for signal transport with minimal losses seems to be construction of the detector modules using long WLS fibers, which had a long attenuation length approaching 6m.

CHAPTER 6 - CONCLUSIONS

The KOPIO reaction ($K_L^0 \rightarrow \pi^0 \nu \bar{\nu}$) is an exceedingly rare, CP-violating decay. Measurement of the branching ratio of this decay could prove to be the most accurate measurement of the CP-violation parameter of the Standard Model. Screening of the “incorrect” decays requires a veto detection system capable detecting charged particles as well as gammas, and must be operational inside a magnetic field. Part of this system has been designed here at Virginia Tech.

The gamma veto detector modules, consisting of alternating layers of lead and plastic scintillator with embedded wavelength-shifting fibers, was found to have a signal strength of approximately 410 photoelectrons per cosmic ray event (9.2 MeV deposited energy per event). The timing resolution was found to be on average 0.7 ns. Analysis of the signal compared to a background spectrum showed no contribution to the signal peak from background. This indicates that the gamma veto modules are adequate for use in the KOPIO detector.

Studies of signal transport methods show that the best means for transporting the signal to the PMTs outside of the magnetic field is to construct the modules using lengths of WLS fiber sufficient to reach the PMTs. Other transport media investigated (Lucite and 5mm square fiber) proved to have an insufficiently long attenuation length, as well as being more physically cumbersome, due to the rigidity of the larger bodies compared to the 1mm-diameter fiber.

REFERENCES

- [1] <http://www.bnl.gov/rsvp/>
- [2] Y.G. Kudenko et. al., *Extruded plastic counters with WLS fiber readout*, *Nuclear Instrumentation Methods*. **A469** (2001) 340
- [3] M. Adams et. al., *A detailed study of plastic scintillating strips with axial wavelength shifting fiber and VLPC readout*, *Nuclear Instrumentation Methods* **A366** (1995) 263, sec.5.1.
- [4] H. Kaspar et. al., KOPIO internal tech-note 29, Nov 2001 (unpublished, <http://pubweb.bnl.gov/users/e926/www/technotes/tn029.ps>).
- [5] S. M. Schonkeren, Eidhoven, “*Photomultipliers*”, the Netherlands April 1970; E.H. Bellamy et. al., *Absolute calibration and monitoring of a spectrometric channel using a photomultiplier*, *Nuclear Instrumentation Methods* **A339** (1994) 468.
- [6] O. Mineev et. al., *Photon sandwich detectors with WLS fiber readout*, *Nuclear Instrumentation Methods* **A494** (2002) 362;
- [7] A.P. Ivashkin et. al., *Scintillation ring hodoscope with WLS fiber readout*, *Nuclear Instrumentation Methods* **A394** (1997) 321.
- [8] See for example the *MINOS Conceptual design report*, Section 5.4.2 “*Fibers*” (unpublished, http://www-numi.fnal.gov/minwork/info/tdr/mintdr_5.pdf).